

**Paper**

# Fundamental Processes of Corona Discharge

## —Surface Analysis of Traces Stained with Discharge on Brass Plate in Negative Corona—

Kanako SEKIMOTO\* and Mitsuo TAKAYAMA\*,<sup>1</sup>

(Received August 20, 2008; Accepted February 10, 2009)

The surface profile and chemical components of the trace stained with negative corona discharge on the brass plate have been analyzed with surface profiler and laser desorption/ionization mass spectrometry, respectively. The trace pattern was made up of several concentric circles and the pattern seemed to reflect the distribution of inhomogeneous electric field strength between point-to-plane electrodes. The surface profile of the trace showed a concave pattern like a crater. Abundant  $\text{NO}_x^-$  and their complexes with Cu were observed in the center region of the crater, while abundant carbon cluster ions  $\text{C}_n^-$  ( $n=2-10$ ) and  $\text{NO}_x^-$  related ions were observed in the rim region of the crater. The results obtained indicated that  $\text{NO}_x^-$  ions were mainly produced on the field line arising from the needle tip apex with high electric field strength, while the periphery of the needle tip with lower field strength resulted in the carbon cluster ions.

### 1. Introduction

Corona discharge has been used as an ionizer in a wide range of research and industrial fields such as environmental, analytical and atmospheric sciences, and possibly even commercial electric appliances. In mass spectrometry, recent atmospheric pressure ionization (API) techniques, e.g., direct analysis in real time (DART)<sup>1)</sup>, atmospheric-pressure solids analysis probe (ASAP)<sup>2)</sup> and charge assisted laser desorption/ionization (CALDI)<sup>3)</sup>, contain corona discharge devices to supply the charge for ionization. Unique application for these ionization techniques is the direct detection of chemicals on surfaces without requiring sample preparation, such as wiping or solvent extraction. The API techniques have demonstrated success in sampling hundreds of chemicals, drugs in abuse, explosives and toxic industrial chemicals on various surfaces such as asphalt, human skin, surfaces of fruits and vegetables, and clothing. Therefore, the API techniques using corona discharge are extremely useful for the rapid, noncontact analysis of substances on surfaces, liquids and gases<sup>1-3)</sup>.

Despite substantial recent progress of the API techniques, the elementary processes involved in ion formation occurring in atmospheric pressure corona

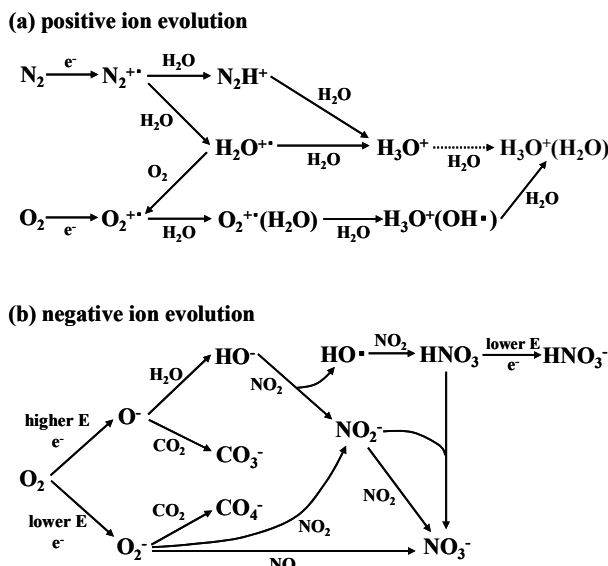
discharge are not yet well understood. Primary ions such as  $\text{N}_2^{+\cdot}$ ,  $\text{O}_2^{+\cdot}$ ,  $\text{O}^-$  and  $\text{O}_2^-$  produced in corona discharge move along the electric field line between the electrodes. Simultaneously, they alter more stable ion species called terminal ions or lose the charge through a number of collisions with common air constituents and by-products of discharge because the mean free path of air (66.3 nm) is very short. Terminal ions generated via successive ion-molecule reactions have few reactive collisions during the majority of their lifetimes and can exist stably in air. A series of ion-molecule reactions from primary to terminal ions have been reported as ion evolutions in both positive and negative corona discharge under atmospheric pressure conditions (Scheme 1)<sup>4-6)</sup>. Negative ion evolution is so complex compared with positive ion, because the sequence of ion-molecule reactions would be controlled by trace gases such as  $\text{CO}_2$  and  $\text{NO}_x$  in air. The studies of corona discharge reported so far show that negative ion evolution is quite complex and that it is difficult to regulate the formation of specific negative ion species.

We have recently established an atmospheric pressure corona discharge system coupled with a mass spectrometer that successfully leads to regular and reproducible generation of positive and negative core ions  $\text{X}^+$  and  $\text{Y}^-$  and their hydrated cluster ions  $\text{X}^+(\text{H}_2\text{O})_n$  and  $\text{Y}^-(\text{H}_2\text{O})_n$ <sup>6)</sup>. The positive cluster ions  $\text{H}_3\text{O}^+(\text{H}_2\text{O})_n$  with core ion  $\text{H}_3\text{O}^+$  were dominantly observed under any conditions in positive corona discharge, in

**Key Words:** corona discharge, brass plate, negative corona, surface profile, chemical components

\* International Graduate School of Arts and Sciences, Yokohama City University, 2-2 Seto, Kanazawa-Ku, Yokohama 236-0027, Japan.

<sup>1</sup> takayama@yokohama-cu.ac.jp



Scheme 1 Sequential progress of (a) positive and (b) negative ion evolutions in corona discharge under atmospheric pressure conditions. Higher and lower E represent the kinetic energy of electrons emitted from the needle tip.

agreement with other previous studies<sup>4,5)</sup>. The mass spectrum of the positive cluster ions  $\text{H}_3\text{O}^+(\text{H}_2\text{O})_n$  ( $n=3-88$ ) is shown in Fig. 1a. The abscissa of the mass spectrum represents mass-to-charge ratio ( $m/z$ ) of ions and the vertical axis indicates relative ion abundance. In the case of negative corona, it was found that various different negative core ions  $\text{Y}^-$  were generated according to the needle voltage and that the needle voltage could be related to the lifetimes of ions<sup>6)</sup>. The lowest corona voltage resulted in the dominant formation of hydroxide core ion  $\text{HO}^-$  with a lifetime of  $10^{-3}$  s, whereas other core ions such as  $\text{NO}_x^-$  and  $\text{CO}_x^-$  with longer lifetimes ( $> 1$  s) were produced at higher needle voltage. Fig. 1b and c show the mass spectra consisting of the dominant negative cluster ions  $\text{HO}^-(\text{H}_2\text{O})_n$  ( $n=3-88$ ) and  $\text{NO}_3^-(\text{H}_2\text{O})_n$  ( $n=0-40$ ), respectively. It is reasonable to consider that the phenomena regarding negative corona discharge would be understood from the standpoint of inhomogeneous electric field strength on the needle tip, because the electric field strength affects the production of primary ions and discharge by-products such as neutral  $\text{NO}_x$  which are significantly involved in the ion evolution to form typical negative core ions  $\text{HO}^-$ ,  $\text{NO}_2^-$ ,  $\text{NO}_3^-$ ,  $\text{HNO}_3^-$ ,  $\text{CO}_3^-$  and  $\text{CO}_4^-$  as shown in Scheme 1b. Therefore, further study of the influence of the field

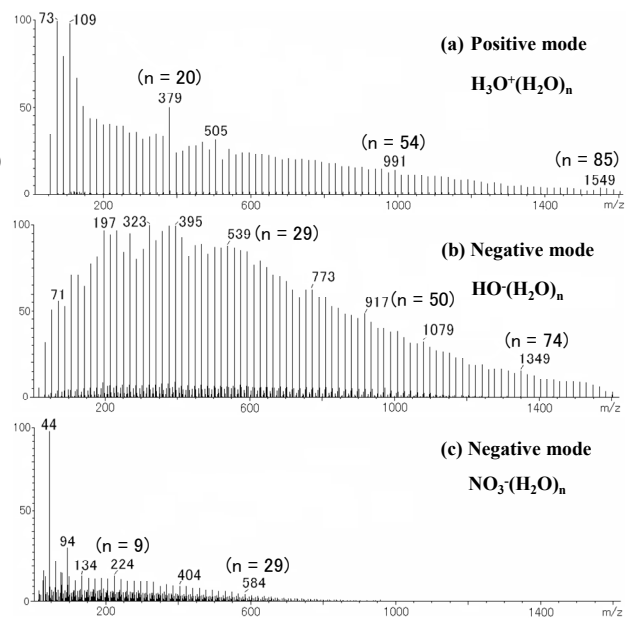


Fig. 1 Corona discharge mass spectra of ambient air. (a) Water cluster ions  $\text{H}_3\text{O}^+(\text{H}_2\text{O})_n$  observed in positive mode, (b)  $\text{HO}^-(\text{H}_2\text{O})_n$  observed in negative mode at low corona voltage, and (c)  $\text{NO}_3^-(\text{H}_2\text{O})_n$  observed in negative mode at high corona voltage.

strength on the formation of negative ions would contribute towards the understanding of the ion evolutions occurring in corona discharge.

Here we attempt to trace the negative ions produced in negative corona discharge on the plate electrode and to analyze the traces stained with discharge on the plate surface, by using microscope, surface profiler and laser desorption/ionization (LDI) mass spectrometry.

## 2. Experimental

### 2.1 Atmospheric pressure corona discharge

The corona discharge device used here consisted of point-to-plane electrodes under ambient air with relative humidity of 50 % and 24°C. The corona needle as a point electrode used was an insect pin with headless (Shiga, Tokyo, Japan), made of stainless steel with a diameter of 200  $\mu\text{m}$  and 20 mm in length. The needle tip with glossy surface was ca. 1  $\mu\text{m}$  in the radius of curvature and the shape of the tip surface was adequately approximated in the form of hyperboloids of revolution (Fig. 2a). The needle was located perpendicular to the brass plate (0.1 mm thick) with a gap of 3 mm (Fig. 2b). Discharge voltage and irradiation time were -4.0 kV and 15 min, respectively.

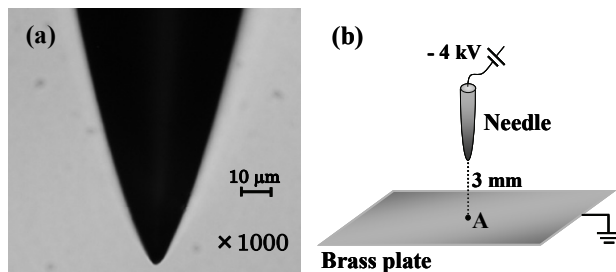


Fig. 2 (a) The optical micrograph of the needle tip used and (b) a configuration of the point-to-plane electrodes.

## 2.2 Microscope, surface profiler and laser desorption/ionization mass spectrometry

Optical micrographs and surface profile of the trace stained with discharge on the plate were obtained by using a BX51 optical microscope (OLYMPUS, Tokyo, Japan) and an Alpha-Step IQ surface profiler (KLA-Tencor, San Jose, CA, USA), respectively. LDI mass spectra were acquired on an AXIMA-CFR instrument (Shimadzu Corp, Kyoto, Japan). A nitrogen laser (337 nm) was used to irradiate and ionize the components of the trace stained with discharge on the plate. The laser beam profile on the target was 200  $\mu\text{m}$  in diameter. The mass spectra were obtained with negative-ion reflectron mode. The acceleration potential was set to 20 kV using a gridless-type electrode. The ion source and analyzer were maintained at  $10^{-5}$  Pa.

(KLA-Tencor, San Jose, CA, USA), respectively. LDI mass spectra were acquired on an AXIMA-CFR instrument (Shimadzu Corp, Kyoto, Japan). A nitrogen laser (337 nm) was used to irradiate and ionize the components of the trace stained with discharge on the plate. The laser beam profile on the target was 200  $\mu\text{m}$  in diameter. The mass spectra were obtained with negative-ion reflectron mode. The acceleration potential was set to 20 kV using a gridless-type electrode. The ion source and analyzer were maintained at  $10^{-5}$  Pa.

## 3. Results and discussion

### 3.1 Traces stained with discharge on the brass plate in negative corona

Figure 3 shows an optical micrograph of the trace stained on the brass plate. The stained trace pattern consisting of several concentric circles with the point A was observed. The center A was the intersection point with the needle axis (Fig. 2b). The stained trace pattern obtained here seems to reflect the electric field distribution between point-to-plane electrodes and the inhomogeneous field strength on the needle tip surface.

If it is assumed that the needle tip used here is shaped in the form of hyperboloids of revolution around  $y$  axis ( $y > 0$ ) and the brass plate is located at the  $x-z$  plane ( $y = 0$ ), according to the method of Eyring *et al.*<sup>7)</sup> the coordinate  $(x(v,u), y(v,u))$  of two-dimensional

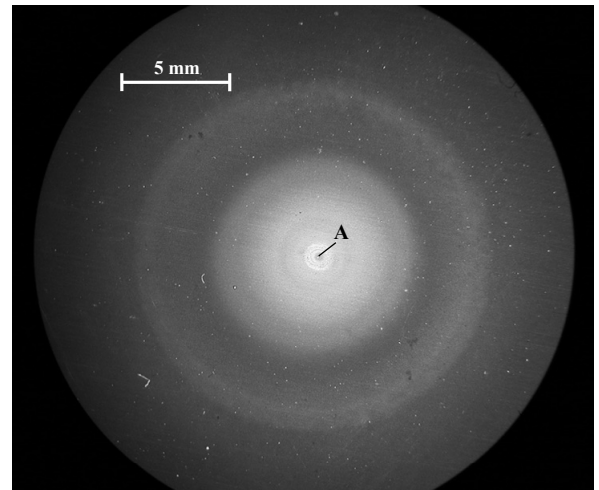


Fig. 3 The optical micrograph of the trace stained with discharge on the brass plate.

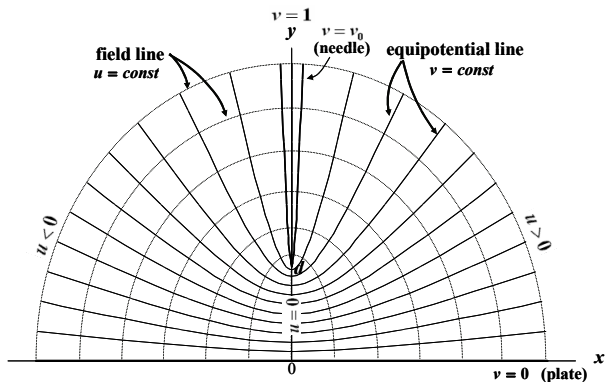


Fig. 4 The coordinate system in  $x-y$  plane representing electric field distribution between a plane and a perpendicular needle by a gap of  $d$ .

electric field between point-to-plane electrodes by a gap of  $d$  m and the electric field strength on the needle tip surface  $E(u)$   $\text{Vm}^{-1}$  are given as follows:

$$x(v,u) = \frac{d}{v_0} u (1 - v^2)^{1/2}, \quad y(v,u) = \frac{d}{v_0} v (u^2 + 1)^{1/2}$$

$$E(u) = -\frac{v_0}{d} \left( \frac{1 - v_0^2}{u^2 - v_0^2 + 1} \right)^{1/2} \cdot \frac{\Phi_0}{\log \frac{1 + v_0}{1 - v_0}} \cdot \frac{1}{1 - v_0^2}$$

A set of hyperboloids for constant  $v$  ( $0 \leq v \leq 1$ ) and an orthogonal set of half ellipses for constant  $u$  ( $-\infty \leq u \leq +\infty$ ) represent equipotential and field lines, respectively. The variables  $\Phi_0$  and  $v_0$  represent the potential difference between the electrodes and a parameter accounting for the characteristic of a hyperbola corresponding to the contour of the cross-sectional needle tip as an equipotential surface, respectively. In the case of

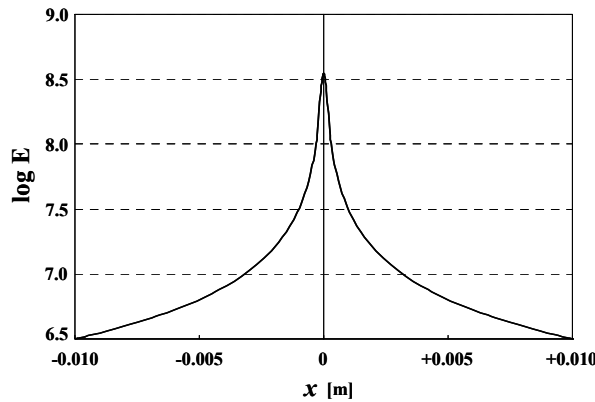


Fig. 5 The calculated electric field strength on the needle tip surface as a function of  $x$  axis on the plate.

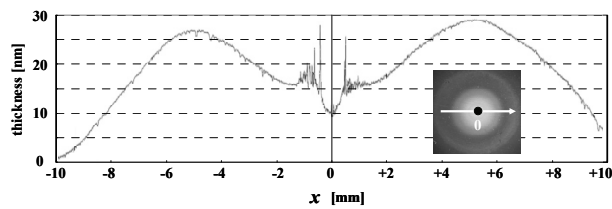


Fig. 6 Uneven surface profile of the trace deposited on the plate surface. Vertical axis represents the thickness of the deposits on the plate.

the experimental conditions here  $v_0$  is 0.99955. The coordinate system in  $x-y$  plane and the calculated field strength distribution on the needle tip as a function of  $x$  axis on the plate are shown in Fig. 4 and Fig. 5, respectively. Three-dimensional coordinate can be obtained by revolution about the  $y$  axis of two-dimensional coordinate. It should be noted that the terminal positions of field lines arising from each position  $u$  on the needle tip correspond to the pattern of concentric circles on the plate. It can be deduced, therefore, that the trace stained on the plate here is produced by the interaction between surface materials on the plate and terminal negative ions generated via ion evolution occurring on each field line. That is, the deposits or products in the center region (point A in Fig. 3) are originating from the negative ions produced on the field line arising from the needle tip apex with the highest field strength ( $u=0$  in Fig. 4), while those in the outer regions are attributed to negative ions moved along field lines arising from lower field strength ( $u \neq 0$  in Fig. 4).

### 3.2 Analysis of the trace stained on the plate

In order to obtain a detailed information on the relationship between the inhomogeneous electric field strength on the needle tip surface and the resulting trace

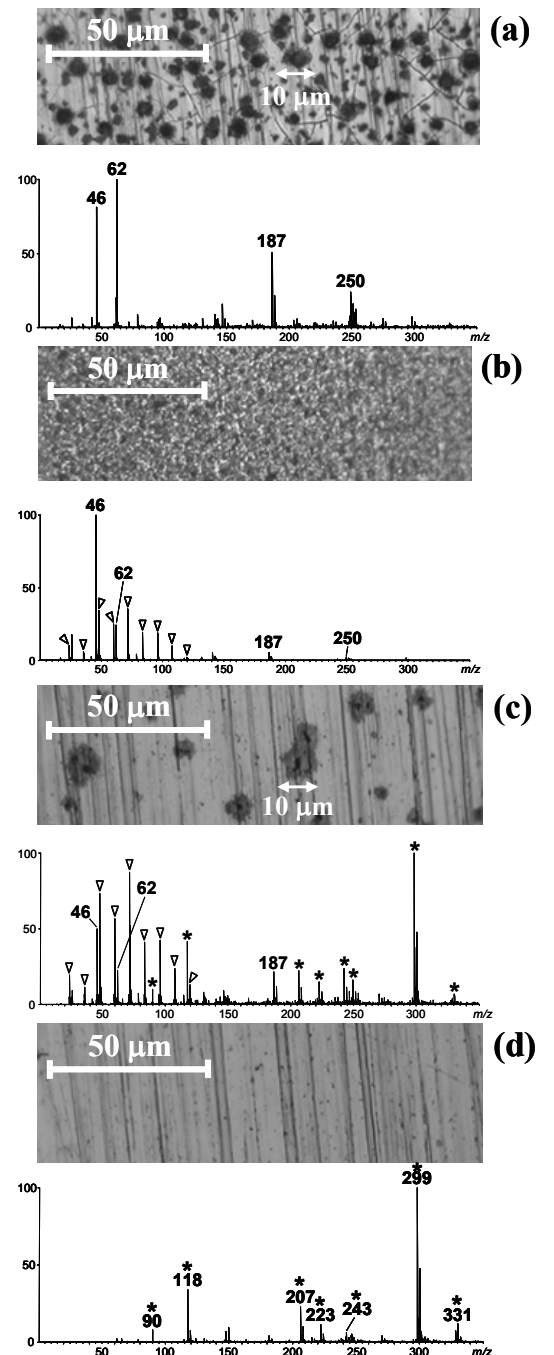


Fig. 7 The optical micrographs and LDI mass spectra of the traces stained with (a) the highest field strength at  $x=0$  mm, (b) relatively high field strength at  $x=+3.0$  mm, (c) low field strength at  $x=+7.0$  mm and (d) without discharge. Asterisk indicates the ions originated from the brass plate. Those ion peaks could not be identified.

stained or deposited on the plate, the surface of the trace was analyzed with surface profiler, microscope and LDI mass spectrometry. Fig. 6 shows the surface profile of the trace deposited on the plate. The optical micrographs and LDI mass spectra for the traces obtained by the highest field strength at  $x=0$  mm, relatively high field strength ( $x=+3.0$  mm) and low field strength ( $x=+7.0$  mm) on the

Table 1 Negative ion species observed in the traces stained with discharge on the plate and corresponding  $m/z$  values

Ion species	$m/z$
$C_n^-$ (n=2-10)	12n
$NO_2^-$	46
$NO_3^-$	62
$NO_3^-(NO_3)Cu$	187
$NO_3^-(NO_3)Cu_2$	250

needle tip and for brass plate as a blank are shown in Fig. 7. Taking into account the laser beam profile on the target with a diameter of 200  $\mu m$ , each LDI mass spectrum obtained here seems to be consisting of the components traced on the whole area of the plate shown in the micrograph. The deposit at the center region attributed to particularly high field strength at  $x=0 \sim \pm 0.5$  mm was thinner than that at outer region originated from lower field strength at  $x=\pm 0.5 \sim \pm 6.0$  mm, as shown in Fig. 6. The chemical components of deposit at the center region were identified as  $NO_x^-$  and complexes of  $NO_x^-$  with Cu as summarized in Table 1. The negative ion species  $NO_x^-$  are well-known as terminal stable negative ions in air and were dominantly observed at higher needle voltage<sup>6)</sup>. The detection of complexes of  $NO_x^-$  with Cu and the observation of cracks on the center region at  $x = 0$  mm (see the micrograph of Fig. 7a) suggested that the surface was coated with the products resulted from the interactions between abundant  $NO_x^-$  and surface materials such as Cu. The mass spectrum obtained over the range at  $x=\pm 0.5 \sim \pm 5.0$  mm showed the peaks corresponding to  $NO_x^-$  and carbon cluster ions  $C_n^-$  (n=2-10,  $\nabla$  in Fig. 7b). The abundances of  $NO_x^-$  and their complex ions decreased with increasing the distance from the center at  $x = 0$  mm. Simultaneously, carbon cluster ions and other ion peaks originated from brass plate relatively increased as shown in Fig. 7c. The increase in distance from the center means the decreasing of the field strength on the needle tip.

The results obtained here indicated that abundant  $NO_x^-$  species were produced on the field line originated from the needle tip apex with high field strength, while in the lower field strength regions the products deposited on the plate were carbon cluster ions  $C_n^-$  as the terminal negative ions. These facts were in agreement with the previous report that the generation of  $NO_x^-$  was promoted

with increasing the electric field strength on the needle tip<sup>6)</sup>.

#### 4. Conclusions

Negative ions produced in negative corona discharge were deposited on the brass plate as an electrode. The surface profile and chemical components of the trace stained with the discharge on the plate were analyzed with surface profiler and laser desorption/ionization mass spectrometry, respectively. The trace pattern was made up of several concentric circles that seemed to reflect the distribution of inhomogeneous electric field strength between point-to-plane electrodes. The surface profile of the trace showed a concave pattern like a crater. The chemical components of the trace in the center of the crater were abundant  $NO_x^-$  and the complexes of  $NO_x^-$  with Cu, while those in the rim of the crater were abundant carbon cluster ions  $C_n^-$  (n=2-10),  $NO_x^-$  and  $NO_x^-$  complexes with Cu. In order to examine the detailed relationships between the field strength and resulting negative ions, the field strength and its distribution on the needle tip were calculated. Calculated field strength and the experimental results here indicated that the abundant  $NO_x^-$  ions were produced on the field line arising from the apex of the needle tip with high electric field strength, while lower field strength in the periphery of the needle tip resulted in the deposit consisting of the carbon clusters. The  $HO^-$  ion and any complexes of  $HO^-$  were not observed in the any traces.

This work was supported by Research Fellowships of the Japan Society for the Promotion of Science for Young Scientists (No.20·10498) and National Institute for Materials Science Nanotechnology Support Network (project ID:AC20035).

#### References

- 1) R.B. Cody, J.A. Lamamee and H.D. Durst: *Anal. Chem.*, **77** (2005) 2297
- 2) C.N. McEwen, R.G. McKay and B.S. Larsen: *Anal. Chem.*, **77** (2005) 7826
- 3) K. Jorabchi, M.S. Westphall and L.M. Smith: *J. Am. Soc. Mass Spectrom.*, **19** (2008) 833
- 4) M. Pavlic and J.D. Skalny: *Rapid Commun. Mass Spectrom.*, **11** (1997) 1757
- 5) K. Turney and W.W. Harrison: *Spectrochim. Acta B*, **61** (2006) 634
- 6) K. Sekimoto and M. Takayama: *Int. J. Mass Spectrom.*, **261** (2007) 38
- 7) C.E. Eyring, S.S. Macheown and R.A. Millikan: *Phys. Rev.*, **31** (1928) 900